(Preprint) AAS 22-061

Attitude Profile Reference for the Earth Orbit Raising Phase of NASA Gateway's Co-Manifested Vehicle

Bradley Humphreys,[1,*] Christine Schmid,[1,*] Michael Martini,[1,*] Melissa McGuire,[1,†] Kurt Hack,[1,‡] Steven McCarty,[1,†] Matthew Holub,[2,§] Nino Tarantino,[2,¶] and Blake Leiker[2,**]

[1]*NASA Glenn Research Center*
Cleveland, OH, 44135, USA
[2]*CACI NSS, Inc*
Houston, TX, 77058, USA

ABSTRACT

As part of NASA's lunar exploration Artemis program, the agency is designing a Gateway to orbit near the moon and provide long term support of a sustained lunar presence at the moon's south pole. The first element launched for the Gateway is the Co-Manifested Vehicle (CMV), comprised of the Power and Propulsion Element (PPE) and Habitation and Lunar Outpost (HALO). The PPE Mission Design team of McGuire & et. al (2021) has developed a Design Reference Mission (DRM) trajectory for CMV's Earth Orbit Raising (EOR) mission phase, which provides the vehicle's 3 degrees of freedom (DoF) trajectory information during the approximately yearlong spiral out from low Earth orbit and into the lunar near-rectilinear halo orbit (NRHO). In tandem, the PPE GN&C team is developing a high-fidelity and fine temporal resolution 6DoF model of the CMV spacecraft's GN&C performance for delivery to the Gateway team; this work acts to bridge the gap between Mission Design's 3DoF reference and GN&C's detailed attitude simulation.

1. INTRODUCTION

The first permanent elements of NASA's Artemis program are Gateway's Power and Propulsion Element (PPE) and Habitation and Logistics Outpost (HALO). After completion, these two elements will be launched as a co-manifested vehicle (CMV), which will then make its way to cis-lunar space where they will stay in orbit about the Earth-Moon's L2 Lagrange point. The CMV will provide resources in cis-lunar space for the other elements of Gateway, primarily power and the propulsion necessary to maintain the lunar orbit (provided by the PPE) and crew quarters (provided by HALO). By slowly building up the Gateway in cis-lunar space prior to crewed missions, the required capability of each element is reduced, while still satisfying Artemis's goal of long-term human presence on the lunar surface. Logistically, the crewed Orion will not have to transport all the equipment necessary

* PPE GNC V&V, Mission Architecture and Analysis Branch
† PPE Mission Design, Mission Architecture and Analysis Branch
‡ PPE Systems Engineering, Mission Architecture and Analysis Branch
§ Johnson Spaceflight Center, Spacecraft Software Engineering Branch
¶ Johnson Spaceflight Center, Simulation and Graphics Branch
** Johnson Spaceflight Center, Guidance Navigation and Control Analysis Branch

for sustained orbit, and each uncrewed element can utilize fuel optimal transportation methods from the Earth to cis-lunar space, as time of flight is not critical.

The CMV, an uncrewed element, will primarily utilize electric propulsion to slowly raise the orbit's perigee over the course of nearly 12 months known as the Earth orbit raising phase (EOR). During this transfer, spacecraft subsystems such as propulsion, thermal, communications, and power all require information on the vehicle's attitude profile over the long duration spiral out to ensure directionally dependent components are correctly pointed. As such, the GN&C subsystem must be capable of controlling the vehicle in a manner that is consistent with the requirements of the mission.

Beginning the attitude constraint problem with propulsion, the CMV's attitude must ensure that PPE's solar electric propulsion engines are aligned to the desired thrust vector provided in the Mission Design's reference trajectory. The thrust direction constrains the vehicle's attitude in 2DoF of rotational freedom, but leaves the rotation of the vehicle about the thrust direction unconstrained to balance thermal, communications, and power pointing requirements.

Unfortunately, the ideal attitudes for the thermal, communications, and power subsystems either directly compete with each other, or result in sub-optimal control scenarios. For example, it has been identified that optimal alignment of the vehicle for thermal considerations can drive maneuvers resulting in excessive use of the vehicle's reaction wheels. This issue occurs because the ideal thermal attitude leads to strict kinematic conditions, requiring the vehicle to perform relatively fast roll maneuvers. By loosening the constraints to allowable vehicle thermal attitude bands (as opposed to optimal bands), it is possible to significantly decrease momentum storage. Additionally, it is desirable to maximize solar power through steering so to keep the vehicle's solar array axis normal to the sun vector. It is also desirable to reduce the momentum storage required by the vehicle's reaction wheels in an attempt to minimize the number of momentum wheel desaturation events, which require additional propulsive maneuvers that subtract from the propellant budget.

While the ideal method of generating the attitude profile would include analytic integration of the state (both translation and orientation) in a way that satisfies the pointing constraints in the system, this approach is infeasible due to the competing pointing constraints listed above. Luckily, the state dynamics are not particularly complicated. The propulsive forces are continuous low-thrust, the shape of the orbit is roughly circular, and the majority of the design reference mission (DRM) takes place beyond the effects of atmospheric disturbances. As a result, it is not strictly necessary to provide a continuous attitude profile for the entire DRM or to use step-wise explicit integration methods (a years worth in this case) required by shooting optimizations; instead collocation methods can be utilized where a set of constraints are satisfied at a fixed number of points with large intervals along the trajectory. The benefit being collocation methods allows for rapid evaluation and generation of attitude profiles while still maintaining dynamic consistency between the nodes.

Using constraint information provided by subsystems, in coordination with vehicle attitude performance capabilities as well as the dynamical governing equations, a 6DoF reference attitude profile has been generated. The attitude profile has been generated by minimizing momentum storage and maximizing solar incidence on arrays while respecting constraints imposed by thermal attitude limits and actuating all necessary control within the vehicles attitude control torque capabilities.

2. HARDWARE

The PPE is a rectangular prism with two large rectangular solar arrays extending in opposition from two of the long panels as seen in Figure 1. The primary body-fixed coordinate frame is the

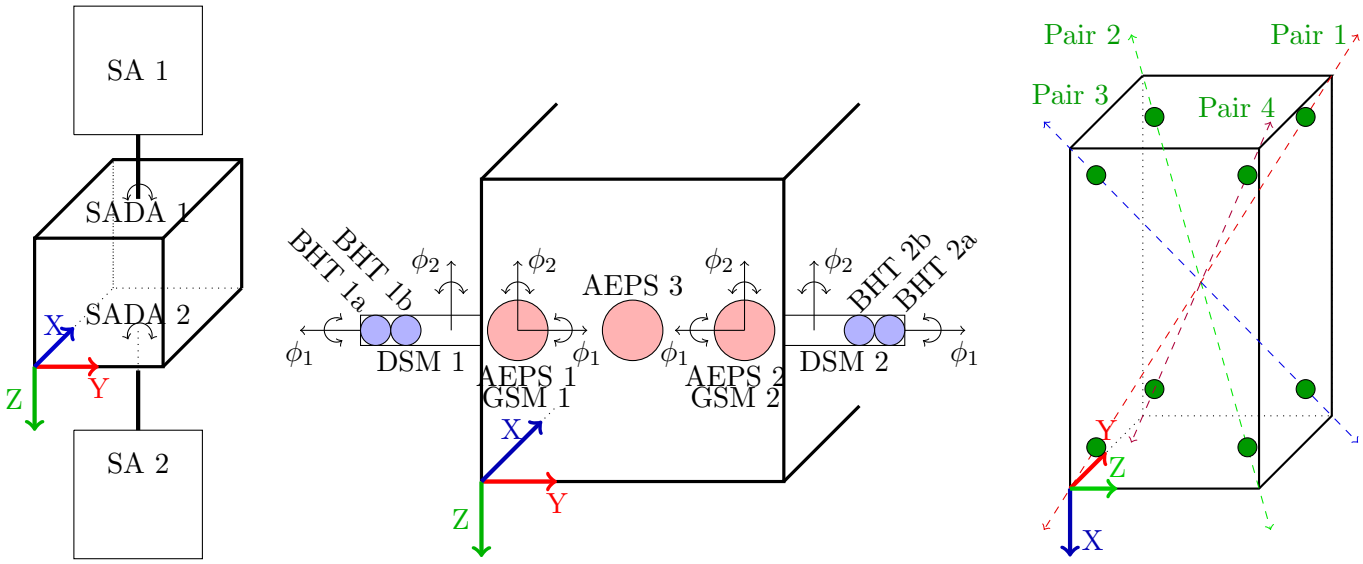

Figure 1. From left to right: the approximate layouts of the NASA Gateway Coordinate System orientation, the thrusters on the propulsion deck with gimbal axes, and reaction wheel torque vectors. Note the orientation of the bus in the reaction wheel image has been rotated and the coordinate frame indicates only orientation of the frame and not the location of the coordinate system's origin.

NASA Gateway Coordinate System (GACS) which is oriented such that the X_{GW}-axis lies along the long axis of PPE and points away from the prop deck, the $-Z_{GW}$-axis points through the solar array nominally oriented "north" in inertial space during NRHO operations, and the Y_{GW}-axis completes the right-handed system. While the true location of the GACS is centered on the $+X_{GW}$ PPE panel (at the PPE/HALO docking interface), the coordinate frame in Figure 1 has been shifted in an attempt to improve readability.

2.1. *Electric Thrusters*

During the EOR portion of the CMV's mission, the primary mode of propulsion comes from four Buesek Hall thrusters (BHT) and three Advanced Electric Propulsion System (AEPS) thrusters collectively denoted as the solar electric propulsion (SEP) thrusters. Due to the low-thrust high-impulse nature of electric propulsion, the thrusters fire nearly continuously with the associated implication that the net thrust vector must be pointed along the required target thrust direction.

The four BHTs (shown in blue in Figure 1) are grouped into two pairs where each pair is mounted on a dual axis stationary plasma thruster module (DSM). DSM1 and DSM2 are attached to the body on the $\mp Y_{GW}$ panels, respectively, near the propulsion deck such that when they are deployed, the BHT plume is clear of the propulsion deck. The DSMs are capable of articulating about the Y_{GW} axis and into/out of the $X_{GW}Z_{GW}$ plane.

All three AEPS thrusters (shown in red in Figure 1) are mounted on the aft prop deck with one mounted in the center and the other two on the edges of the prop deck such that all three are colinear and aligned with the Y_{GW} axis. The central AEPS thruster is hard mounted to the prop deck while the other two are mounted via gimbaled solar electric propulsion modules (GSMs) which allow each thruster to be gimbaled about the Z_{GW} axis (toward/away from each other) and into/out of the $X_{GW}Y_{GW}$ plane.

Gimballing of the thrusters ensures the net thrust vector from the collective SEP thrusters either passes through the vehicle's center of mass for varying mass properties or is offset to manage the vehicle's momentum.

2.2. *Reaction Wheels*

Nominally, the pointing constraints imposed by the SEP sysetm and the solar arrays are satisfied using four pairs of reaction wheels oriented such that the eight total wheels provide full 3DoF attitude control. For this study, it is assumed that all eight wheels remain functional and that each wheel is capable of spinning at $\pm$5000 rpm (i.e. both clock and counterclockwise) with a corresponding momentum of 208 Nms.

The reaction wheels can be desaturated using torque offsets from SEP gimbaling, "feathering" the solar arrays, aligning the bus to induce torque on the body from solar radiation pressure, or firing of the 3DoF chemical reaction control thrusters.

2.3. *Solar Arrays*

The solar arrays are the singular means of power generation on the PPE; therefore, it is crucial that the arrays are oriented such that they are continuously illuminated. The solar arrays are attached to the PPE $\pm Z_{GW}$ panels and are rotary driven by Solar Array Drive Assemblies (SADA). To ensure enough power is generated for nominal operations during EOR, the incidence angle between the face of the solar panels and the sun vector is minimized.

3. MISSION DESIGN AND OPERATIONS

During EOR, it is desirable to minimize the use of reaction control system propellants by minimizing the frequency of reactions wheel desaturations. Through the use of momentum management with the wheels, solar arrays, and possibly SEP steering, the frequency of desaturations can be minimized. Additional operational considerations include maximizing sun incidence on the solar arrays (for power and thermal considerations) and minimizing the vehicle thrust vector deviation from mission trajectory targets provides the information necessary to produce a desired attitude corridor[1]. Strict adherence to this corridor can drive high momentum usage; therefore, the goal of this work is to generate an attitude profile that best satisfies the various attitude and performance constraints imposed on the vehicle.

Three figures of merit are used in the optimization cost function:

- minimization of the reaction wheel torque across the trajectory epoch,
- maximization of the solar incidence on the solar arrays across the trajectory epoch, and
- maximization of the alignment of the thrust vector to the target across the trajectory epoch.

The PPE Mission Design team generates an EOR Design Reference Mission (DRM) that utilizes ground rules and assumptions to investigate performance trades in achieving mission goals. Trades such as propellant usage, Earth to Moon transfer time, and eclipse timing/duration are considered. The optimization is performed using the Copernicus (NASA JSC (2021)) software package, and a reference 3DoF trajectory is selected and provided to the spacecraft subsystem designers. While the

[1] Results from this work are being used to flush out other attitude constraints i.e. communication

DRM provides a rich output of relevant trajectory information, the items relevant to this analysis are:

- Vector (x/y/z): Position of the Spacecraft in Earth Centered J2000 Frame, [2]
- Vector (x/y/z): Position of the Spacecraft in Sun Centered J2000 Frame,
- Vector (x/y/z): Thrust Vector in J2000 Inertial Frame, and
- Combined Thrust level for SEP.

Using this information the following can be calculated:

- Unit vector of the Earth's position with respect to the PPE expressed in J2000 inertial frame: $\hat{\boldsymbol{r}}^{J2K}_{ppe,earth}$,
- Unit vector of the Sun's position with respect to the PPE expressed in J2000 inertial frame: $\hat{\boldsymbol{r}}^{J2K}_{ppe,sun}$,
- Unit vector of spacecraft thrust in J2000 inertial frame: $\hat{\boldsymbol{F}}^{J2K}_{thrust}$, and
- Thrust level of individual engines (with assumptions of distribution across engines): F_{aeps1}, F_{aeps2}, F_{aeps3}, F_{bht1a}, F_{bht1b}, F_{bht2a}, and F_{bht2b}

One possible analysis scenario is to constrain the vehicle's thrust line to the prescribed thrust direction. This locks two of the vehicle's rotational degrees of freedom leaving only the roll about the thrust axis free. To satisfy the power constraints, the roll degree of freedom can then be constrained by requiring the vehicle's solar array axis to be perpendicular to the sun vector, arriving at a completely kinematic, fully-constrained solution. This straight-forward profile actually produces an excessive momentum usage problem; when the sun vector becomes nearly co-linear with the vehicle thrust axis, the vehicle must perform 180° "snap" or "keyhole" rolls as seen in Figure 2. There are two solutions for the roll angle that will keep the vehicle array axis perpendicular to the sun vector. The solutions are mirrored about the vehicle's X-Z plane. This means at the inflection point, it is possible for the vehicle to roll to the other solution. The work herein will be used to help support the investigation of the optimal parameters for these targeting algorithms.

4. MODEL

The goal is to formulate the dynamics of the vehicle as a set of first order equations of motion, define state variables, and define input control trajectories so that the system can be transcribed into a direct collocation framework. The equations of motion were developed symbolically in analytical closed form. Kinematic transformations were used to describe each of the subsystem's momentum, then the torque was calculated using symbolic differentiation. While the kinematic transformations are tedious, use of energy methods such as Lagrange or Kane's was not required. This is because the vehicle is a body with attached rotating appendages (body with eight reaction wheels and two solar arrays).

[2] Unless specified otherwise, such as here, the coordinate system used throughout is a coordinate system with its origin at the vehicle center of mass and aligned to the GACS coordinate frame

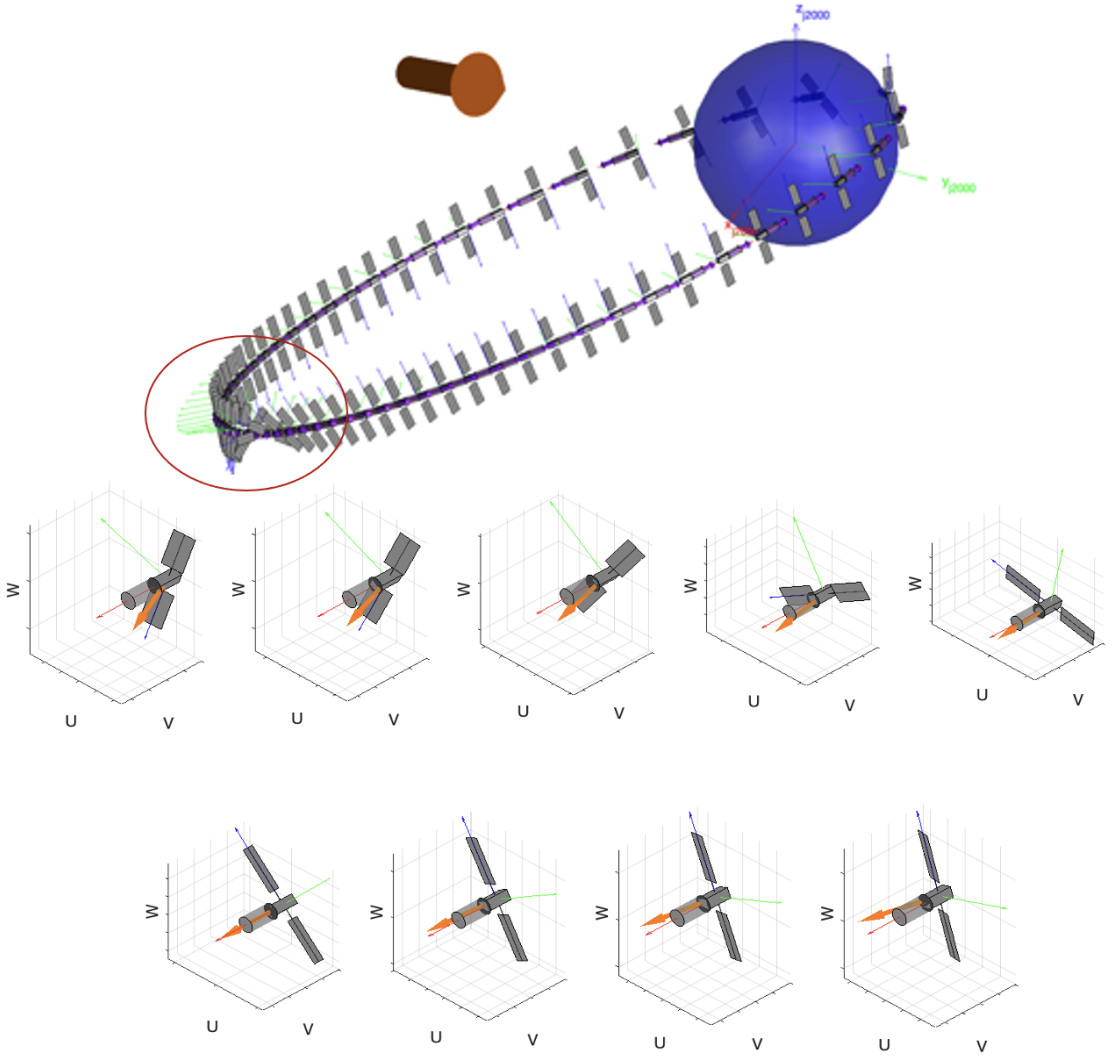

Figure 2. Example CMV Orbit. Orange Arrow is Sun Vector. Successive frames below show area of interest: the sun vector nearly aligning to vehicle X axis and causing a "snap" roll

The vehicle attitude dynamics are modeled as a sum of moments about its center of mass in the vehicle body frame. The body frame is located at the vehicle's center of mass and is aligned to the GACS. The vehicle mass and location of the center of mass is currently considered to be fixed throughout the entirety of the flight. The equation of motion for the vehicle is:

$$\mathbf{I_{veh}} \begin{bmatrix} \dot{\omega}_{veh,x} \\ \dot{\omega}_{veh,y} \\ \dot{\omega}_{veh,z} \end{bmatrix} = \mathbf{T_{RW}} + \mathbf{T_{SA}} + \mathbf{T_{SEP}} \,, \tag{1}$$

where $\mathbf{I_{veh}}$ is the vehicle's inertia tensor and the right hand side of the equation is the sum of torques due to the reaction wheels, solar arrays, and electric thrusters respectively.

4.1. *Reaction Wheel Model*

The reaction wheel torque ($\mathbf{T_{RW}}$) on the body is the sum of the 8 reaction wheels' torque mapped into the vehicle body frame. The location and orientation of the eight wheels results in four unique

torque vectors. As a result, the reaction wheels operate in four pairs, implying their momentum and torque can also be combined into four pairs. The torque equations were derived from the sum of the reaction wheel momentum and include Coriolis effects. The detailed derivation is not shown here, but the four wheel pairs exert:

$$\mathbf{T_{RW}} = \sum_{i=1}^{4} f_{rw,i}(\omega_{rw,i},\ \dot{\omega}_{rw,i},\ \omega_{veh,x},\ \omega_{veh,y},\ \omega_{veh,z},\ \dot{\omega}_{veh,x},\ \dot{\omega}_{veh,y},\ \dot{\omega}_{veh,z}) \tag{2}$$

Later we will want to limit the reaction wheels' acceleration based on their torque motor capabilities, so we describe their torque-speed relationship as:

$$\dot{\omega}_{rw,1} = \frac{T_{rwmotor,1}}{I_{rw}} \tag{3}$$

$$\dot{\omega}_{rw,2} = \frac{T_{rwmotor,2}}{I_{rw}} \tag{4}$$

$$\dot{\omega}_{rw,3} = \frac{T_{rwmotor,3}}{I_{rw}} \tag{5}$$

$$\dot{\omega}_{rw,4} = \frac{T_{rwmotor,4}}{I_{rw}} \tag{6}$$

Equations (3)-(6) are first order differential equations. Variables are classified as follows:
State Variables:

- Reaction Wheel Angular Velocity: $\omega_{rw,1}$ through $\omega_{rw,4}$
- Vehicle Angular Rates (Body frame): $\omega_{veh,x}$, $\omega_{veh,y}$, and $\omega_{veh,z}$

Unknown Trajectories:

- Reaction Wheel Motor Torque: $T_{rwmotor,1}$ through $T_{rwmotor,4}$

4.2. *Solar Array Model*

The solar array torque ($\mathbf{T_{SA}}$) on the body is the sum of the solar array rotation torque mapped into the vehicle body frame. The torque equations were derived from the sum of the array momentum and also include Coriolis effects. Each of the solar arrays exerts:

$$\begin{aligned}\mathbf{T_{SA}} =& f_{sa,1}(\omega_{sa,1},\ \dot{\omega}_{sa,1},\ \omega_{veh,x},\ \omega_{veh,y},\ \omega_{veh,z},\ \dot{\omega}_{veh,x},\ \dot{\omega}_{veh,y},\ \dot{\omega}_{veh,z}) + \\ & f_{sa,2}(\omega_{sa,2},\ \dot{\omega}_{sa,2},\ \omega_{veh,x},\ \omega_{veh,y},\ \omega_{veh,z},\ \dot{\omega}_{veh,x},\ \dot{\omega}_{veh,y},\ \dot{\omega}_{veh,z})\end{aligned} \tag{7}$$

We will want to limit the solar array angular acceleration based on the actuator torque capabilities, so we describe their torque-speed relationship as:

$$\dot{\omega}_{sada,1} = \frac{T_{sadamotor,1}}{I_{SA,rot}(\theta_{sada,1})} \tag{8}$$

$$\dot{\omega}_{sada,2} = \frac{T_{sadamotor,2}}{I_{SA,rot}(\theta_{sada,2})} \tag{9}$$

Equations (8) and (9) are first order differential equations. The two state variables are $\omega_{sada,1}$ and $\omega_{sada,2}$. The inputs will be $T_{sadamotor,1}$ through $T_{sadamotor,2}$.

The solar arrays have non-negligible inertia. Therefore, their inertias needs to be factored into the vehicle inertia:

$$\mathbf{I_{veh}}(\theta_{sada,1}, \theta_{sada,2}) = \mathbf{I_{veh,base}} + \mathbf{I_{SA}}(\theta_{sada,1}, \theta_{sada,2}) \tag{10}$$

where $\mathbf{I_{veh,base}}$ is the inertia of the bus excluding the solar arrays. This requires the addition of two more first order differential equations and state state variables:

$$\dot{\theta}_{sada,1} = \omega_{sada,1} \tag{11}$$

$$\dot{\theta}_{sada,2} = \omega_{sada,2} \tag{12}$$

Variables are classified as follows:

State Variables:

- Solar Array rotation Angle: $\theta_{sada,1}$ and $\theta_{sada,2}$
- Solar Array Angular Velocity: $\omega_{sada,1}$ and $\omega_{sada,2}$
- Vehicle Angular Rates (Body frame): $\omega_{veh,x}$, $\omega_{veh,y}$, and $\omega_{veh,z}$

Unknown Trajectories:

- Solar Array Motor Torque: $T_{sadamotor,1}$ and $T_{sadamotor,2}$

4.3. *Solar Electric Propulsion Model*

In general, the solar electric propulsion system is used to direct the net engine thrust vector through the vehicle's center of mass while the reaction wheels perform steering to follow the prescribed trajectory. During EOR, the SEP engines are generally not throttled and are at prescribed thrust settings. It is, though, to thrust slightly off the center of mass due to: 1) an inaccurate center of mass position location (among other kinematic uncertainties) used in gimbal positioning calculations or 2) to help with vehicle momentum management. Using the SEP to perform momentum management though would come at inefficiency of maintaining the prescribed thrust vector to meet mission planning. The SEP system was therefore modeled as a sum of force vectors around the vehicle center of mass.

The torques from the SEP are then:

$$\begin{aligned}\mathbf{T_{SEP}} = {} & f_{T,aeps1}(\theta_{aeps1,1}, \theta_{aeps1,2}, F_{aeps1}) + f_{T,aeps2}(\theta_{aeps2,1}, \theta_{aeps2,2}, F_{aeps2}) + f_{T,aeps3}(F_{aeps3}) + \\ & f_{T,bht1a}(\theta_{dsm1,1}, \theta_{dsm1,2}, F_{bht1a}) + f_{T,bht1b}(\theta_{dsm1,1}, \theta_{dsm1,2}, F_{bht1b}) + \\ & f_{T,bht2a}(\theta_{dsm2,1}, \theta_{dsm2,2}, F_{bht2a}) + f_{T,bht2b}(\theta_{dsm2,1}, \theta_{dsm2,2}, F_{bht2b})\end{aligned} \tag{13}$$

and the forces are:

$$\begin{aligned}\mathbf{F_{SEP}} = {} & f_{F,aep1}(\theta_{aeps1,1}, \theta_{aeps1,2}, F_{aeps1}) + f_{F,aep2}(\theta_{aeps2,1}, \theta_{aeps2,2}, F_{aeps2}) + f_{F.aep3}(F_{aeps3}) + \\ & f_{F,bht1a}(\theta_{dsm1,1}, \theta_{dsm1,2}, F_{bht1a}) + f_{F,bht1b}(\theta_{dsm1,1}, \theta_{dsm1,2}, F_{bht1b}) + \\ & f_{F.bht2a}(\theta_{dsm2,1}, \theta_{dsm2,2}, F_{bht2a}) + f_{F,bht2b}(\theta_{dsm2,1}, \theta_{dsm2,2}, F_{bht2b})\end{aligned} \tag{14}$$

Variables are classified as follows:

State Variables:

- None Introduced

Unknown Trajectories:

- Engine Gimbal Angles: $\theta_{aeps1,1}$, $\theta_{aeps1,2}$, $\theta_{aeps2,1}$, $\theta_{aeps2,2}$, $\theta_{dsm1,1}$, $\theta_{dsm1,2}$, $\theta_{dsm2,1}$, and $\theta_{dsm2,2}$

Known Trajectories:

- Engine forces (from design reference mission): F_{aeps1}, F_{aeps2}, F_{aeps3}, F_{bht1a}, F_{bht1b}, F_{bht2a}, and F_{bht2b}

4.4. *Attitude Model*

The vehicle body states are in terms of angular velocity in the body frame while the thrust direction, the sun vector, and Earth vector are all in the J2000 inertial frame. Therefore, we need to integrate the vehicle rotation to get a transformation of the inertial vectors into the body frame. To do this we will utilize a quaternion for the rotation of the vehicle relative to the inertial frame. Using the definition of the first two quaternion derivatives:

$$\dot{\mathbf{q}} = \frac{1}{2}\mathbf{\Omega}(\omega)\mathbf{q} \tag{15}$$

$$\ddot{\mathbf{q}} = \frac{1}{4}\mathbf{\Omega}(\omega)\mathbf{\Omega}(\omega)\mathbf{q} + \frac{1}{2}\dot{\mathbf{\Omega}}(\dot{\omega})\mathbf{q} \tag{16}$$

where for a Hamiltonian (scalar last) quaternion, $\mathbf{\Omega}(\omega)$ is the skew-symmetric matrix:

$$\mathbf{\Omega}(\omega) = \begin{bmatrix} 0 & \omega_{veh,z} & -\omega_{veh,y} & \omega_{veh,x} \\ -\omega_{veh,z} & 0 & \omega_{veh,x} & \omega_{veh,y} \\ \omega_{veh,y} & -\omega_{veh,x} & 0 & \omega_{veh,z} \\ -\omega_{veh,x} & -\omega_{veh,y} & -\omega_{veh,z} & 0 \end{bmatrix} \tag{17}$$

A 2nd order Taylor series is expressed as:

$$f(x) = f(x_o) + f'(x_o)(x - x_o) + \frac{1}{2}f''(x_o)(x - x_o) \tag{18}$$

Rearranging Equation (18), you can arrive at a backwards finite difference formula for quaternion states:

$$\frac{\mathbf{q_t} - \mathbf{q_{t-1}}}{\Delta t} = \mathbf{q'_t} - \frac{1}{2}\mathbf{q''_t}\Delta t \tag{19}$$

Taking the derivatives denoted by primes in Equation (18) with respect to time and substituting in the discretized forms of Equations (15) and (16) into the first and second derivatives respectively yields:

$$\dot{\mathbf{q}}_{\mathbf{update}} = \frac{\mathbf{q_t} - \mathbf{q_{t-1}}}{\Delta t} = \frac{1}{2}\mathbf{\Omega}(\omega_\mathbf{t})\mathbf{q_t} - \frac{1}{8}\mathbf{\Omega}(\omega_\mathbf{t})\mathbf{\Omega}(\omega_\mathbf{t})\mathbf{q_t}\Delta t - \frac{1}{4}\dot{\mathbf{\Omega}}(\dot{\omega})\mathbf{q_t}\Delta t \tag{20}$$

Equation (20) provides a second-order approximation of the first derivative of the quaternion state. We only need a 2nd order approximation because our model only extends to $\dot{\omega}$ and there are no

higher terms i.e. $\ddot{\omega}$. This is a truncated Taylor series expansion and therefore an approximation that may not produce a unit quaternion. To ensure a unit quaternion we have followed the methodology suggested by Betts (2010) (Section 6.8): we use the first three entries in the quaternion (the vector portion) and do not directly utilize the q_4 scalar. Using a "slack" trajectory allows the scalar to float during integration. This is done using the state equations:

$$\dot{\mathbf{q}}_{\mathbf{att},[\mathbf{1..3}]} = \dot{\mathbf{q}}_{\mathbf{update}[\mathbf{1..3}]} \tag{21}$$

$$\dot{q}_{att,4} = \dot{q}_{4,slack} \tag{22}$$

Then a constraint equation at each node is used to ensure a unit quaternion:

$$q_{att,1}^2 + q_{att,2}^2 + q_{att,3}^2 + q_{att,4}^2 - 1 = 0 \tag{23}$$

State Variables:

- Attitude of the vehicle as a quaternion: $q_{att,1}$, $q_{att,2}$, $q_{att,3}$, $q_{att,4}$

Unknown Trajectories:

- A slack trajectory on the quaternion scaler rate to allow for ensuring a unit quaternion state: $\dot{q}_{4,slack}$

For the objective functions defined later we will need to transform the DRM J2000 based vectors into the vehicle body frame. To do this, the quaternion is transformed into a direction cosine matrix, $\boldsymbol{R}_{J2K}^{Body}$ and then multiplied by the vectors from Mission Design's DRM:

$$\begin{aligned} \hat{\mathbf{r}}_{ppe,earth}^{Body} &= \mathbf{R}_{J2K}^{Body}\ \hat{\mathbf{r}}_{ppe,earth}^{J2K} \\ \hat{\mathbf{r}}_{ppe,sun}^{Body} &= \mathbf{R}_{J2K}^{Body}\ \hat{\mathbf{r}}_{ppe,sun}^{J2K} \\ \hat{\mathbf{F}}_{ppe,thrust}^{Body} &= \mathbf{R}_{J2K}^{Body}\ \hat{\mathbf{F}}_{ppe,thrust}^{J2K} \end{aligned} \tag{24}$$

5. OPTIMIZATION

5.1. *Direct Collocation Overview*

The first step in building a direct collocation problem is to define all of the system states and the equation of motions of those states. They are written out in first order state equations. For example, a linear form would be: $\dot{x}(t) = Ax(t) + Bu(t)$ where x is the state vector and u is the known input trajectories. Typically this explicit equation is solved by integrating over time and may require very small time steps. In direct collocation the problem is broken up into N temporal nodes that are typically larger than integrator step size. A backward finite difference is substituted in place of the state derivatives:

$$\frac{x(t_n) - x(t_{n-1})}{\Delta T} - Ax(t_n) - Bu(t_n) = 0 \tag{25}$$

$$n = 1, 2, ..., N \tag{26}$$

$$\Delta T = \frac{\text{Total Time}}{N} \tag{27}$$

In direct collocation, the optimizer adjusts state values at each node so that Equation (25) is held true. This means the number of states multiplied by the number of nodes are calculated to ensure that the governing state equation(s) hold true. This ensures that the state values at each node lead to a set of states at the next node that also solve the equation(s). This is referred to as dynamic consistency and is posed to an optimizer as a constraint set. There can typically be a large number of solutions that will provide dynamic consistency; therefore, the optimizer is also given a objective function to minimize. For example, the objective function could be to minimize a subset of the states that correspond to body torques or propellant usage.

While direct collocation is a framework to pose a problem, an optimizer is needed to actually find the solution. We are utilizing IPOPT (via cyipopt, Aides et. al. (2021)). which is a gradient based interior point optimizer. It is specifically designed to search for the minimum of large scale (significant free variables) constrained problems. To significantly increase its efficiency in solving a problem, the gradient of the objective function with respect to the free parameters (state's unknown trajectories) should be provided as a function. The same is true for the constraints; a function containing the Jacobian with respect to the free parameters should be provided. The objective gradient and the constraints Jacobian must be continuous. When there are a large number of equations, this can become arduous. Our means of addressing this is to write all of the equations (f_{rw}, $f_{sa,1}$, $f_{sa,2}$, etc.) out symbolically using Python's sympy package (Certik et. al. (2021)). These equations stay in the standard differential equation form. To "transcribe" them to nodal based direct collocation functions we utilized the Opty python package (Moore et. al. (2021), Moore & van den Bogert (2018)). This package generates the constraint and Jacobian functions, compiles it into C code, aggregates all other inputs, and poses the problem to IPOPT.

One word of caution with performing gradient based interior point optimization: there is no guarantee of reaching a global minimum; it is quite possible to achieve a local optimum based upon the chosen initial guess.

5.2. *Problem Definition*

5.2.1. *Equations of Motion*

There are 15 equations of motion:

- 3 from vehicle rotational acceleration: from Equation (1)
- 4 from reaction wheel torque: from Equations (3) - (6)
- 2 from solar array rotational acceleration: Equations (8) and (9)
- 2 from solar array rotational velocity: from Equations (11) and (12)
- 4 from the attitude quaternion rate: from Equations (21) and (22)

The 15 state derivatives and state variables are:

$$\dot{\boldsymbol{y}} = \begin{bmatrix} \dot{\omega}_{veh,x} &= \cdots \\ \dot{\omega}_{veh,y} &= \cdots \\ \dot{\omega}_{veh,z} &= \cdots \\ \dot{\omega}_{rw,1} &= \cdots \\ \dot{\omega}_{rw,2} &= \cdots \\ \dot{\omega}_{rw,3} &= \cdots \\ \dot{\omega}_{rw,4} &= \cdots \\ \dot{\omega}_{sada,1} &= \cdots \\ \dot{\omega}_{sada,2} &= \cdots \\ \dot{\theta}_{sada,1} &= \cdots \\ \dot{\theta}_{sada,2} &= \cdots \\ \dot{q}_{att,1} &= \cdots \\ \dot{q}_{att,2} &= \cdots \\ \dot{q}_{att,3} &= \cdots \\ \dot{q}_{att,4} &= \cdots \end{bmatrix} \iff \boldsymbol{y} = \begin{bmatrix} \omega_{veh,x} &= \cdots \\ \omega_{veh,y} &= \cdots \\ \omega_{veh,z} &= \cdots \\ \omega_{rw,1} &= \cdots \\ \omega_{rw,2} &= \cdots \\ \omega_{rw,3} &= \cdots \\ \omega_{rw,4} &= \cdots \\ \omega_{sada,1} &= \cdots \\ \omega_{sada,2} &= \cdots \\ \theta_{sada,1} &= \cdots \\ \theta_{sada,2} &= \cdots \\ q_{att,1} &= \cdots \\ q_{att,2} &= \cdots \\ q_{att,3} &= \cdots \\ q_{att,4} &= \cdots \end{bmatrix}$$

There are 16 known (input) trajectories in the equations of motion and 15 unknown trajectories:

$$\boldsymbol{r}_{known} = \begin{bmatrix} F_{aeps1} \\ F_{aeps2} \\ F_{aeps3} \\ F_{bht1a} \\ F_{bht1b} \\ F_{bht2a} \\ F_{bht2b} \\ \hat{r}^{J2K}_{ppe,earth,x} \\ \hat{r}^{J2K}_{ppe,earth,y} \\ \hat{r}^{J2K}_{ppe,earth,z} \\ \hat{F}^{J2K}_{thrust,x} \\ \hat{F}^{J2K}_{thrust,y} \\ \hat{F}^{J2K}_{thrust,z} \\ \hat{r}^{J2K}_{ppe,sun,x} \\ \hat{r}^{J2K}_{ppe,sun,y} \\ \hat{r}^{J2K}_{ppe,sun,z} \end{bmatrix} \qquad \boldsymbol{r}_{unknown} = \begin{bmatrix} T_{rwmotor,1} \\ T_{rwmotor,2} \\ T_{rwmotor,3} \\ T_{rwmotor,4} \\ T_{sada,1} \\ T_{sada,2} \\ q_{att,slack,4} \\ \theta_{dsm1,1} \\ \theta_{dsm1,2} \\ \theta_{dsm2,1} \\ \theta_{dsm2,2} \\ \theta_{gsm1,1} \\ \theta_{gsm1,2} \\ \theta_{gsm2,1} \\ \theta_{gsm2,2} \end{bmatrix}$$

5.2.2. *Free Parameters*

The free parameters at node 1 are then:

$$\mathbf{x}_1 = \begin{bmatrix} \mathbf{y}_1 \\ \mathbf{r}_{unknown,1} \end{bmatrix} \tag{28}$$

The result is $30N$ free unique parameters from the combined $\boldsymbol{y}$ and $\boldsymbol{r}_{unknown}$ vectors, which are evaluated at N nodes giving a vector of length $30N$:

$$\mathbf{x} = \begin{bmatrix} \mathbf{y}_1 \\ \mathbf{r}_{unknown,1} \\ \vdots \\ \mathbf{y}_N \\ \mathbf{r}_{unknown,N} \end{bmatrix} \tag{29}$$

5.2.3. *Constraints*

Constraints include:

- Constraints to maintain dynamic consistency of the above equations of motion at every node. ($18N$ constraints)
- At every node, 14 constraints are added by lower and upper bounding the free trajectories: $T_{rwmotor}$, $T_{sadamotor}$, $\theta_{gsm,1}$, $\theta_{gsm,2}$, $\theta_{dsm,1}$, and $\theta_{dsm,2}$. ($14N$ constraints)
- Additionally an instance constraint is placed at every node to ensure the attitude quaternion states are unit normal (N constraints): Equation (23)
- Depending on the simulation being performed, instance constraints at the beginning nodes so as to provide initial conditions that ensure the constraint space are met and the system states are initialized with those that match the DRM. (18 Constraints)
- No constraints are added to the states. This means there is no upper limit on the reaction wheel speeds. This is done to determine the frequency of needing to perform desaturations without having to introduce the discontinuity of RCS firings into the model. For this approximation, it is assumed that the desaturations using reaction control jets are ideal: instantaneous, pure torques, and not disturbing the orbit trajectory. Post simulation the reaction wheel speeds are tracked and whenever a wheel pair exceeds the saturation limit, the wheel speeds are reset and desaturation event count is incremented.

5.2.4. *Objective Function*

We are minimizing a weighted 3 part objective function.

1) **Minimize the reaction wheel torque profile**

First we extract the reaction wheel torque input trajectories ($T_{rwmotor,1}$ ... $T_{rwmotor,1}$) from the free parameters as $\mathbf{x}_{rw1}$ through $\mathbf{x}_{rw4}$. Then we use a minimum effort (sum square) function. The function is normalized by dividing through by the maximum available composite torque of all the reaction wheels on the spacecraft.

$$J_{rw} = \frac{1}{4T_{rw,max}^2}(\mathbf{x}_{rw1}^T\mathbf{x}_{rw1} + \mathbf{x}_{rw2}^T\mathbf{x}_{rw2} + \mathbf{x}_{rw3}^T\mathbf{x}_{rw3} + \mathbf{x}_{rw4}^T\mathbf{x}_{rw4}) \tag{30}$$

2) **Maximize the solar incidence on the arrays**

First we extract the solar angles from the free parameters. Next we calculate the unit vector of the solar array in the body frame: $\hat{\boldsymbol{r}}_{sada}^{Body}$. From equation 24 we have the unit vector of the sun: $\hat{\boldsymbol{r}}_{ppe,sun}^{Body}$. Solar incidence is then calculated as:

$$\phi_n = ((\hat{\boldsymbol{r}}_{sada} \cdot \hat{\boldsymbol{r}}_{ppe,sun}^{Body})^2)^{1/2} \tag{31}$$

where n indicates that this is calculated at each of the N nodes. The square and square root address that either side of the array can be the "active" side; it essentially performs an absolute value operation that has a derivative. The incidence will span from 1 (array normal) to 0 (array perpendicular). As IPOPT attempts to minimize the objective function, $1 - \phi$ is used in the cost function.

The solar arrays are independently gimabled making the objective function a combination of the two solar incidences

$$J_{sa} = \frac{1}{2N}\left(\sum_{n=1}^{N}(1 - \phi_{sada1,n}) + \sum_{n=1}^{N}(1 - \phi_{sada2,n})\right) \tag{32}$$

3) **Maximize the vehicle thrust alignment to that specified in the DRM**

Using the function developed in Equation (14), the unit thrust force is calculated.[3] The alignment angle is then again calculated using the dot product as:

$$\psi_n = \hat{\boldsymbol{r}}_{thrust,n} \cdot \hat{\boldsymbol{F}}_{ppe,thrust,n}^{Body} \tag{33}$$

This can span from 1 (aligned), through 0 (perpendicular), to -1 (opposite direction). To normalize all of the objectives to the domain $0:1$, we use $(\psi_n + 1)/2$. The objective function then becomes:

$$J_{sep} = \frac{1}{N}\sum_{n=1}^{N}\left(\frac{\psi_n + 1}{2}\right) \tag{34}$$

The combined objective function is then:

$$J = w_{rw}J_{rw} + w_{sa}J_{sa} + w_{sep}J_{sep} \tag{35}$$

where w_{rw}, w_{sa}, w_{sep} are constant weighting factors used in exploring the trade space.

6. RESULTS

Results have been generated in sets with intervals approximately 3 months in duration and general qualitative findings are:

1. The solution is very sensitive to objective weighting. This is typical for multi-objective optimization problems.
2. Optimizing over 1-year duration EOR is unneeded and tends to drive an average solution, which was still seen even when breaking the simulation down into 3 month intervals. Instead, breaking the optimization into shorter duration epochs i.e. 7 days, provides more desired solutions. Of course, this is also computationally faster and allows re-tailoring of the weights. It also better reflects actual spacecraft operations which have 7 day planning horizons.

[3] Care must be taken when there are no active SEP thrusters and the implied normalization becomes undefined.

3. There is a greater than expected use of solar array actuator torque (especially during perigee passes) to drive spacecraft steering. While a simplification, when the solar array alignment weighting is relatively lower, the reaction wheels tend to orient the vehicle to allow the more powerful solar array drive motors to torque the vehicle.

To address the first finding, the problem is being restructured to:

1. Convert the thrust alignment into a hard inequality constraint. Setting a maximum allowable thrust misalignment allows for developing a Pareto front and trade momentum versus solar alignment.

2. The same can be done, but restructuring the problem so have a constraint placed on the solar misalignment and trade momentum versus thrust misalignment. This information is of interest to the mission design team as it allows them to better understand misalignment margins that they keep in reserve.

3. Move both the thrust and solar misalignment from the objective function and apply as hard inequality constraints. The objective function would then be fully focused on minimizing reaction wheel torque effort.

7. CONCLUSIONS AND FUTURE WORK

The problem has been formulated in the collocation framework, solved using constrained optimization in Python. It is planned to additionally implement the problem using OpenMDAO with Dymos Falck et al. (2021) to take advantage of Gauss-Lobatto collocation and the Radau Pseudospectral method. This should allow for further decreasing the number of temporal nodes and increase computational efficiency.

8. NOMENCLATURE

Symbol	Name
f_{rw}, f_{sa}	Closed form function mapping reaction wheel or solar array to vehicle dynamics
$f_{F,bht}$, $f_{F,aeps}$	Closed form function for the BHT or AEPS engine forces on the vehicle
$f_{T,bht}$, $f_{T,aeps}$	Closed form function for the BHT or AEPS engine torque on the vehicle
F_{aeps1}, F_{aeps2}, F_{aeps3}	AEPS engine thrust 1, 2, and 3 (scaler)
F_{bht1a}, F_{bht1b}	BHT Engine A and B on DSM 1 thrust (scaler)
F_{bht2a}, F_{bht2b}	BHT Engine A and B on DSM 2 thrust (scaler)
$\hat{\mathbf{F}}^{\mathbf{Body}}_{\mathbf{ppe,thrust}}$	DRM Unit thrust vector on PPE in the vehicle body frame
$\hat{\mathbf{F}}^{\mathbf{J2K}}_{\mathbf{ppe,thrust}}$	DRM Unit thrust vector on PPE in the J2000 coordinate system
$\mathbf{I_rw}$	Reaction Wheel Rotational Inertia (scaler)
$\mathbf{I_veh}$	Vehicle Inertia Tensor (including solar arrays)
$\mathbf{I_veh,base}$	Vehicle Inertia Tensor (without solar arrays)
J	Objective function
J_{rw}, J_{sa}, J_{sep}	Reaction wheel, solar array incidence, and SEP thrust alignment objective functions
$\mathbf{q}$	Unit quaternion
$\mathbf{q_{update}}$	Quaternion update
$q_{att,1}$ .... $q_{att,4}$	Quaternion of vehicle attitude, elements 1 through 4
q_{slack}	Slack quaternion variable
N	Number of collocation nodes
$\mathbf{R}^{Body}_{J2K}$	Rotation matrix from J2000 frame to vehicle body
$\hat{\mathbf{r}}^{\mathbf{Body}}_{\mathbf{ppe,earth}}$, $\hat{\mathbf{r}}^{\mathbf{Body}}_{\mathbf{ppe,sun}}$	Unit vector from PPE to the Earth or the Sun in the vehicle body frame
$\hat{\mathbf{r}}^{\mathbf{J2K}}_{\mathbf{ppe,earth}}$, $\hat{\mathbf{r}}^{\mathbf{J2K}}_{\mathbf{ppe,sun}}$	Unit vector from PPE to the Earth or the Sun in J2000 frame
$\mathbf{T_{RW}}$, $\mathbf{T_{SA}}$, $\mathbf{T_{SEP}}$	Composite torque vector of reaction wheels, solar arrays, and SEP engines on the vehicle body
$T_{rwmotor,1}$, ..., $T_{rwmotor,4}$	Reaction wheel pair 1 through 4 motor torque
$T_{sadamotor,1}$, $T_{sadamotor,2}$	Solar array 1 and 2's SADA motor torque
w_{rw}, w_{sa}, w_{sep}	Objective weighting parameter for the reaction wheels, solar array incidence, and SEP thrust alignment
X_{GW}, Y_{GW}, Z_{GW}	Gateway coordinate system X, Y, and Z Directions
θ_{sada1}, θ_{sada2}	Solar array 1 and 2's rotation angle
$\theta_{XXX\alpha,\beta}$	Engine gimbal angle
– XXX	Indicates which thruster type: AEPS or BHT
– α	Indicates which thruster: AEPS 1, 2, or 3 −− BHT 1a, 1b, 2a, or 2c
– β	Indicates which of the two axes are being gimbaled
ϕ	Solar incidence on panels
ψ	SEP Thrust alignment to DRM
$\omega_{rw,1}$, ..., $\omega_{rw,4}$	Reaction wheel pair 1 through 4 angular velocity

Symbol	Name
$\dot{\omega}_{rw,1}$, ..., $\dot{\omega}_{rw,4}$	Reaction wheel pair 1 through 4 angular acceleration
$\omega_{sada,1}$, $\omega_{sada,2}$	Solar array 1 and 2's SADA angular velocity
$\omega_{veh,x}$, $\omega_{veh,y}$, $\omega_{veh,z}$	Vehicle angular velocity (x,y,z body directions)
$\dot{\omega}_{veh,x}$, $\dot{\omega}_{veh,y}$, $\dot{\omega}_{veh,z}$	Vehicle angular acceleration (x,y,z body directions)

Acronym	Name
AEPS	Advanced Electric Propulsion
BHT	Buesek Hall Thrusters
CMV	Co-manifested Vehicle
DoF	Degree of Freedom
DAPM	Deployment and Positioning Modules
DRM	Design Reference Mission
DSM	DAPM SEP Modules (BHT gimbal mechanism)
EOR	Earth Orbit Raising
GACS	NASA Gateway Coordinate System
GSM	Gimbaled Module (AEPS gimbal mechanism)
GW	Gateway
HALO	Habitation and Logistics Outpost
J2K	J2000 Coordinate System
MD	Mission Design
NRHO	Near-Rectilinear Halo Orbit
PPE	Power and Propulsion Element
RW	Reaction Wheel
RWMOTOR	Reaction Wheel Motor
SA	Solar Arrays
SADA	Solar Array Drive Assemblies
SADAMOTOR	Solar Array Drive Motor
SEP	Solar Electric Propulsion
VEH	Vehicle

Sym.	Name
x	Scaler
$\dot{x}$	Time derivative
$\hat{\boldsymbol{x}}$	Vector of unitary length
$\boldsymbol{x}$	Vector
$\boldsymbol{x}^c_{a,b}$	Vector from a to b in frame c
$\boldsymbol{X}^b_a$	Transformation from frame a to b
$\boldsymbol{X}$	Matrix
x_t	Variable x at time t

REFERENCES

Aides et. al. 2021, cyipopt, v.1.1.0, ,

Betts, J. T. 2010, Practical Methods for Optimal Control and Estimation Using Nonlinear Programmin, 2nd Edition, 2nd edn. (Society for Industrial and Applied Mathematics)

Certik et. al. 2021, sympy, v.1.9, ,

Falck, R., Gray, J., Ponnapalli, K., & Wright, T. 2021, Journal of Open Source Software, 6, 2809

McGuire, M., & et. al. 2021, in 5, Vol. 4, Astrodynamics Specialist Conference, ed. T. editor, AAS/AIAA (Big Sky, MT: The publisher), 213, an optional note

Moore, J. K., & van den Bogert, A. 2018, Journal of Open Source Software, doi:10.21105/joss.00300

Moore et. al. 2021, opty, v.1.1.0, ,

NASA JSC. 2021, copernicus, v.5.1, ,